A NEW ELECTRODE-MESH TOMOGRAPH FOR ADVANCED STUDIES ON BUBBLY FLOW CHARACTERISTICS

Steffen RICHTER

Tokyo Institute of Technology
2-12-1 Meguro-ku, 152-8550 Tokyo, JAPAN

Masanori ARITOMI

Tokyo Institute of Technology
2-12-1 Meguro-ku, 152-8550 Tokyo, JAPAN

Keywords: bubbly flow characteristics, conductive computer tomography, volume flow measurement

ABSTRACT

For studies on the characteristics of bubble flow in a rectangular channel (20x100mm) a new electrode-mesh tomograph have been applied. The measuring principle is based on local conductivity measurement and a signal concerning. The applied sensor scans the local void fraction distribution in 2 parallel planes, separated 1.5mm in flow direction, with a resolution of 3.0x2.2mm and a overall sampling rate of 1200Hz (all 256 points). Algorithm for the calculation of the local instantaneous void fraction distribution and the true gas velocity are presented. Based on these values the approximate shape of bubbles have been reconstructed and the gas volume flow through the sensor evaluated. The superficial gas velocity as well as the local distribution of the gas volume flux can be calculated.
An extensive sensitivity study illustrating the applicability and accuracy is presented, based on experimental observations as well as theoretical considerations.
The evaluated results are compared with high-speed video observations of the flow field as well as data comparing the reconstructed volume flow with measurements by a laminar flow meter. Good agreement can be stated.

INTRODUCTION

For design improvement of nuclear reactors as well as the assessment of their safety features advanced hydrodynamic computer codes have been developed. It is obvious that from the point of CFD code development, there is the necessity to verify the developed models with high quality databases, which were obtained from experiments complementing the resolution of modern CFD codes in spatial and temporal concerns. Intensive studies on the sensitivity of all parameters will supply sufficient knowledge that allows to extrapolate data obtained from (scaled) experiments to the real facility as well as to assess the accuracy of numerical simulation applied to an integral facility.
Several attempts have been made in the past to solve this problem. Remarkable results have been reached by the use of X-ray tomography, which is able to supply data with a resolution in the order of several millimeters and a temporal resolution are in the order of milliseconds. Cited should be Hori et al. [1] who realized a spatial resolution of approximately 2mm by an overall sampling rate of 2000Hz.
Beside of the cost-intensive X-ray technology, attempts have been made be use of intrusive sensors utilizing the measurement of the electrical conductivity. Besides many others, Prasser et al. [4], who used a sensor where 16x16 electrodes were arranged in 2 planes and a temporal resolution of 1024 Hz have been realized, should be cited [4], [5].
Since the approach done by Prasser et al. [4] was considered as outstanding by the authors in terms of temporal and spatial resolution, the aim has been to use this kind of sensor for studies on flow characteristics for bubbly flow in a comparatively narrow channel of 20x100mm cross-section. Beside the local, instantaneous void fraction distribution there have been particular interest in measuring the local true velocity of the dispersed phase, the approximate bubble size as well as their distributions and to calculate from the obtained data the superficial gas velocity as well as to conclude to the distribution of the volume flux.

SENSOR DESCRIPTION

The used sensor was developed and manufactured at the FZR Research Center Rossendorf, Institute of Safety Analysis, Dresden, Germany, and is similar to the device reported by Prasser et al. [4]. An illustration of the applied device is given by Fig.1.

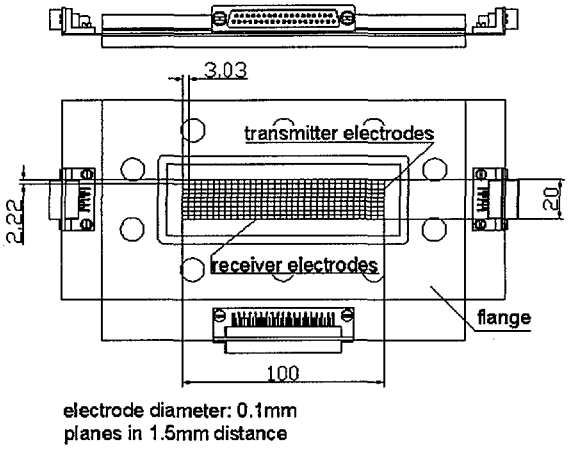

Figure 1 – Layout of the electrode-mesh tomograph, WMT

Design

The electrode-mesh sensor, WMT, was designed to cover the entire channel cross-section of 20x100mm size. The normal vector on the cross-section and the channel length coordinate are parallel. 2x8x16 electrodes are spread out crosswise (90°) in 3 planes. Two planes, each containing 8 parallel equidistant electrodes, work as receiver planes, whereby one plane, centered between the two receiver planes, works as transmitter plane. Each plane is separated 1.5mm so that the measured conductivity is an integral value of the fluid properties in an ancient region around the crossing point along this 1.5mm separation distance of the electrodes. The fact that the electrode planes are parallel two planes of points result (up- and downstream the transmitter plane), where the conductivity of the fluid is evaluated and which are further referred as measuring planes containing points with the coordinates (x_1,x_2). Since transmitter as well as receiver electrodes are arranged equidistant, an effective spatial resolution of 2.2 x 6.1mm results. With a wire diameter of 0.1mm, a free cross-section of 96% remains.

The sensor is mounted in flanges fitting the size of the experimental apparatus.

An overall sampling rate of 1200Hz have been realized with the available hardware (1 sample = 2 measuring planes, each containing 128 measuring points).

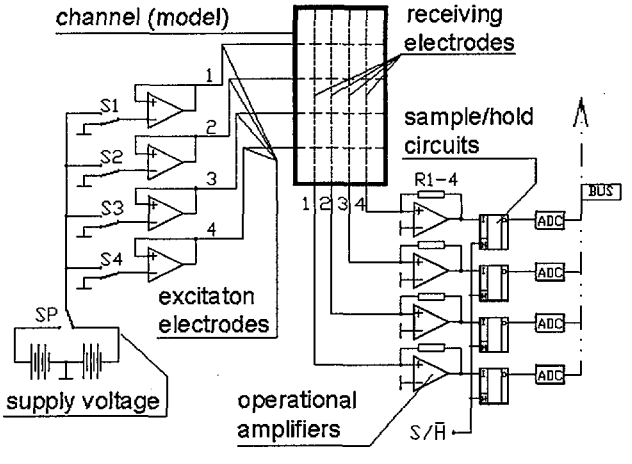

Figure 2 – Simplified electrical scheme,[5]

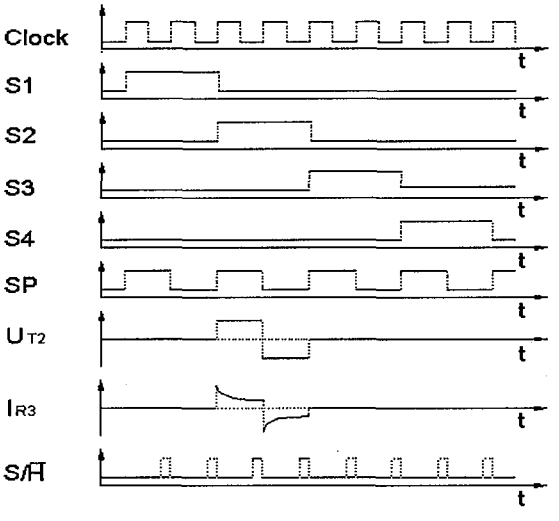

Figure 3 –Simplified control sequence, [5]

Control concept and signal acquisition

A simplified electric scheme of the WMT is illustrated in Fig.2. Transmitter wires are successively activated by a multiplex circuit closing the switches S1-S4. To avoid electrolysis the potential on the temporarily activated transmitting wire is inverted once in each half excitation-period by switching SP that yields a supplied voltage on the electrodes, which is rectangular in shape, as illustrated by

U_{T2} in Fig.3. The excitation of a transmitter wire causes a current in the receiving wire (e.g. I_{R3} in Fig.3). Since all receiver wires are scanned separately, each crossing point of transmitter and receiver electrodes is scanned individually. The resulting current is transformed into voltage by operational amplifiers (R1-R4 in Fig.3) and kept by sample/hold circuits. To distinguish between the current that is caused by the influence of the capacity around the scanned crossing point and current that is a function of the local conductivity, the sample/hold circuits are released by the switch S/H after a stable voltage level is reached (Fig.3). The released signal is 12 bit AD converted and stored by a data acquisition computer.
The general possibility of cross-talk between the electrodes is avoided by applying an impedance to the output of the transmitters as well as the input of the receivers, significantly lower than the impedance of the fluid. This keeps the potential of all non-activated electrodes to zero [4]. A proposal by Prasser et al. [4] have been followed for the conversation from measured conductivity values to the local void fractions, assuming a linear dependency of the local void fraction from the conductivity. So the instantaneous local void fraction $\varepsilon(t)$ at the point (x_1, x_2) writes for a constant current supplied by the amplifier, [4]:

$$\varepsilon(t)_{X1,X2} = \frac{(U_{el}(t))_{X1,X2} - (U_{el}(t)^W)_{X1,X2}}{(U_{el}(t)^A)_{X1,X2} - (U_{el}(t)^W)_{X1,X2}} \qquad (1)$$

The assumption of a linear dependency between the local void fraction and the induced current is a simplification used and has to be understood as approximation in 1st order. The obtained quality for void fraction measurements were found to be accurate by 1% in comparison to X-ray tomography [4]. To assure that the correct values for U_{el}^A and U_{el}^W are used (the case of only Air, Water, respectively), the sensor is calibrated before every experiment.

METHODS FOR FURTHER DATA PROCESSING

The measured void fraction writes in general form:

$$\varepsilon = \varepsilon(\vec{r},t) \qquad (2)$$

and is characterized by a spatial resolution of 2.2 x 6.1mm and a resolution in time of 0.83ms. It have been verified that the measured void fraction is within 1% exact [4]. Based thereon, the general possibility to obtain more advanced data of flow characteristics by use of the available sensor have been investigated. In particular, about the local true gas velocity as well as the possibility for spatial reconstruction of the flow field was thought. The study was limited to pure co-current bubbly flow of an air-water mixture at atmospheric pressure and ambient temperature. The superficial velocity of the water did not exceed 25cm/s and the geometry of the channel have been chosen to 20x100mm.

Local true gas velocity, Basic

The measurement of the local instantaneous true gas velocity is based on the analysis of the time a bubble migrates from one point on one measuring plane to the peripheral measuring point of the opposite plane.
If the bubble enters an ancient region around the crossing point, the void fraction signal $\varepsilon(t)$ changes from zero to a larger level, as illustrated by Fig.4. This ramp, $\Phi_{\varepsilon,pos}$, can be expressed at a point $\vec{r}$:

$$\Phi_{\varepsilon,pos}(\vec{r},t) = (\varepsilon(\vec{r},t) = 0) \cap (\varepsilon(\vec{r},t+dt) > 0) \qquad (3)$$

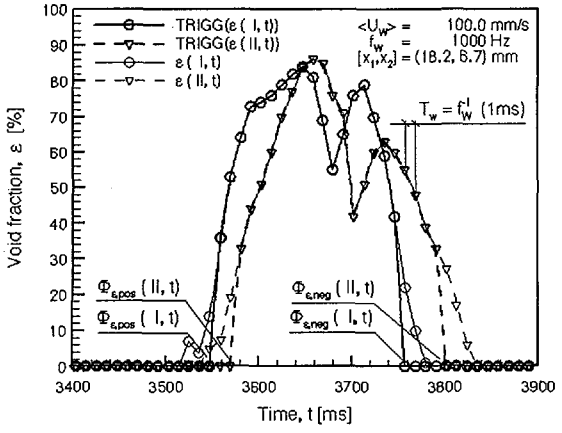

Figure 4 – Example of converted void fraction signal

So the velocity of the bubble is defined as the surface velocity of the approaching interfacial area. Considering also the negative ramp, $\Phi_{\varepsilon,neg}$, yields less accurate data. The reason is seen in a temporal alteration of the bubble shape by the wires, which results in a non-neglectable difference between the surface velocity and the volume-averaged rising velocity. This effect can also be seen by the void fraction course illustrated in Fig.4, where the signal obtained by the downstream plane II is slightly elongated. Due to the same fact former approaches, utilizing a time correlation function for the evaluation of the local gas velocity failed, since the character of bubble deformation is statistically not randomly distributed.

If two ramps Φ_ε occur, separated by the vector $\vec{s}$, the delay time Δt between these events allows to conclude the average surface velocity within the distance $|\vec{s}|$:

$$\Delta t : \Phi_{\varepsilon,pos}(\vec{r},t) \cap \Phi_{\varepsilon,pos}(\vec{r}+\vec{s},t+\Delta t) \qquad (4)$$

To ensure that identified ramp events result from the migration of one and the same continuously by the gas occupied volume, Eq.(4) have been extended:

$$\Delta t : \Phi_{\varepsilon,pos}(\vec{r},t) \cap \Phi_{\varepsilon,pos}(\vec{r}+\vec{s},t+\Delta t) \cap [\varepsilon(\vec{r},t+\Delta t) > 0] \qquad (5)$$

The use of the delay time Δt for the evaluation of the surface velocity u in the described way implies that there is a maximum measurable velocity u_{max} for an overall sampling frequency f_W and the distance between the measuring planes Δ_W:

$$u_{max} = \Delta_W \cdot f_W \qquad (6)$$

Any object moving faster than u_{max} and large enough to be detected by both measuring planes would be identified as migrating with the maximum velocity u_{max}. Slower objects yield a measurable delay time that can be expressed in terms of delay frames δ (i.e. number of overall samples):

$$u_\delta = \frac{\Delta_W \cdot f_W}{\delta} \qquad (7)$$

, which is characterized by a measuring uncertainty between u_δ and $u_{\delta+1}$:

$$U_\delta = \frac{\Delta_W \cdot f_W}{\delta(\delta+1)} \qquad (8)$$

The true velocity u: $u_\delta < u \leq u_{\delta+1}$ remains unknown. Further it is obviously that the p.d.f. for the delay-time appears algebraically stretched if it is plotted over velocity arguments.

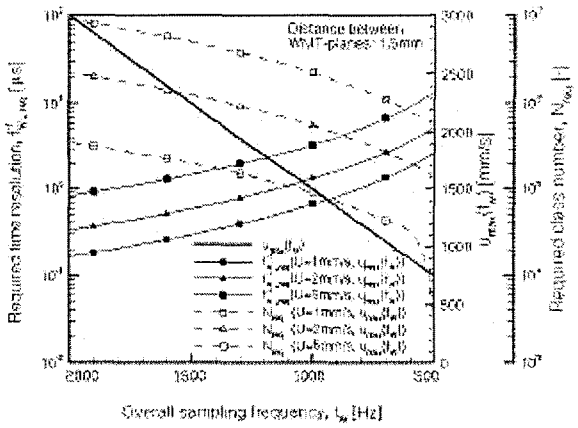

Figure 5 – Comparison, realized and required temporal resolution

In Fig.5 a comparison between the realized overall sampling frequency f_W, the corresponding maximal measurable velocity u_{max} and the required time resolution $f_{w,req}^{-1}$ is shown for aimed uncertainties in the velocity evaluation U_δ of 1,2 and 5mm/s. The graph proceeds assumes Δ_W = 1.5mm. Obviously, the required temporal resolution f_W is about 1 order higher for a given maximum velocity u_{max} than the present available hardware is able to realize.

However, considering the mentioned uncertainty in velocity measurement with mathematical rigor besides the feature being able to supply detailed information about the instantaneous void fraction distribution were promising enough to make an approach toward the defined aim.

Local true gas velocity, approach

In general, the statistical characteristic of the delay time Δt between two (positive) ramp events $\Phi_{\varepsilon,pos}(\vec{r},t)$ and $\Phi_{\varepsilon,pos}(\vec{r}+\vec{s},t+\Delta t)$ are determined by a p.d.f. p_T:

$$p_T = \frac{\partial P(\Delta t < T)}{\partial \Delta t} \tag{9}$$

Sufficient high time resolution supposed, the delay-time mean value $E(\Delta t)$ gives directly the statistically expected velocity of the gaseous phase E(U).

The uncertainty in the velocity measurement, Eq.(8), yields that evaluated velocities u: $u_\delta < u \leq u_{\delta+1}$ are accumulated at the measurable velocities $u_{\delta+1}$. However, the number of detected events belonging to a velocity class U_δ, as defined by Eq.(8), is constant, independent if all events appears to be accumulated at a velocity u_δ within U_δ or if they are distributed by a distribution function $\tilde{\tilde{p}}_u$ over U_δ. With the discreet distribution function $\tilde{\tilde{p}}_u$ (which is sufficient to serve the requirements in time-resolution and normalized in U_δ), the velocity distribution function p_u can be replaced by a new distribution function $\tilde{p}_u$.

The probability $P(\Delta t < T)$, or correspondingly $1-P(u<U)$, can so be expressed either by the measurable velocity classes U_δ or by the redistributed velocity classes $\tilde{U}_i$:

$$\sum_{\{\delta\}} p_{u\delta} U_\delta = \sum_{\{j\}} \tilde{p}_{uj} \tilde{U}_j = \sum_{\{\delta\}} \sum_{\{k\}} \tilde{\tilde{p}}_{uk} p_{u\delta} U_\delta \tag{10}$$

with:

$$\sum_{\{\delta\}} U_\delta = \sum_{\{j\}} \tilde{U}_j \tag{11}$$

The spectrum of local gas velocities in bubbly flow does not show any singularities and behaves smooth since the velocity fluctuation of a single bubble around the time averaged value have been found as distributed with steady function, [2],[3],[6]. Facing this point, an approach in 1st order can be legitimized by assuming that the frequency of all true velocities u within one measurable velocity class U_δ are equally distributed and so $\tilde{\tilde{p}}_u$ is constant over U_δ.

The PDF $\tilde{\tilde{p}}_u$ is normalized within U_δ:

$$\sum_{\{U_\delta\}} \tilde{\tilde{p}}_{uk} = 1 \tag{12}$$

The redistribution of the N_δ velocity classes that are larger in class-width U_δ than the required class-width $\tilde{U}_k$ writes for temporal equidistant sampling cycles δ:

$$N_\delta < N_j : p_{u\delta} U_\delta = p_{u\delta} \sum_{\{k\}} \tilde{\tilde{p}}_{uk} \tilde{U}_k \tag{13}$$

With:

$$U_\delta = \sum_{\{k\}} \tilde{U}_k \tag{14}$$

The statistical moments are altered slightly if an assumption for the statistical behavior of the bubble rising velocities within the uncertainty is made by introduction of $\tilde{\tilde{p}}_u$. The mean value E(u) and the standard deviation $D^2(u)$ are of particular interest:

$$E(u) = \int_{u=0}^{\infty} u \cdot f(u) du = \sum_{j=1}^{\infty} \tilde{p}_{Uj} \cdot \tilde{U}_j \tag{15}$$

$$D^2(u) = \int_{u=0}^{\infty} (U - E(u))^2 f(u) du = \sum_{j=1}^{\infty} \tilde{p}_{Uj} (\tilde{U}_i - E(u))^2 \tag{16}$$

The results obtained by application of the proposed algorithm are discussed in the section 'Test results and comparison'.

Phase reconstruction

The algorithm for the velocity measurement supplies information about the statistically expected local true gas velocities in a two-phase mixture. Simultaneously, the local void fraction is measured.

With these information an approximate reconstruction of the bubble shape and its volume can be carried out. This idea have been first reported by Prasser et al. [4] and is based on the localization of a volume continuously filled with gas, which is appropriately clustered.

The algorithm proposed by Prasser et al. [4] has the disadvantage that the volumetric flux is supposed to be constant over the cross section. This simplification is not further necessary since the local instantaneous true gas velocity, u_G, have been, Eqs.(9)-(16).

To evaluate the area in A_c, which is occupied by the gaseous phase at a certain time t, and to repeat the process for all t till the entire structure is clustered, a list $L\varepsilon$ is introduced:

$$\begin{aligned} L\varepsilon &= [\varepsilon(\vec{r}_1,t_1),\varepsilon(\vec{r}_2,t_2),....\varepsilon(\vec{r}_n,t_n)]^T \\ &= [\varepsilon((x_1,x_2)_1,t_1),\varepsilon((x_1,x_2)_2,t_2),....\varepsilon((x_1,x_2)_n,t_n)]^T \end{aligned} \qquad (17)$$

This list $L\varepsilon$, given by Eq.(17), contains all local instantaneously measured values of the void fraction that resulting from the same bubble structure. It have been found by extensive studies on single bubbles and bubble collectives that there exists a unique value of ε, ε_{thresh}, which is a certain identifier that a gas structure is in between these points. The value is independent from the cross-sectional averaged void fraction and slightly altered by bubble rising velocity (+/-5% for rising velocities between 200~500mm/s). This threshold have been set to ε_{thresh}=10% and is kept constant for every flow condition. The void fraction signal have been triggered by ε_{thresh} and in the following only this triggered signal, noted with ε, is considered. Using this triggered signal ε, it has been avoided to jump during the scan procedure from one bubble to the next, except for situation where two bubble are shortly before coalescence, which corresponds to a cross sectional void fraction of about 10%. A qualitative criteria to assess, if a certain instantaneous void fraction distribution over A_c is caused either by 2 small bubbles, which are closed before coalition, or by 1 larger structure have been found: If the clustered $\varepsilon(x_1,x_2,t)$-field shows more than one local maximum, it is supposed that there exist more than a single bubble. This case is important for the correct evaluation of the bubble diameter. The local gas volume flux distribution is not influenced.

The proposed utilized clustering procedure can be expressed by the recursive formula noted below:

$$\begin{aligned} L\varepsilon_i^{k+1}\begin{pmatrix}\tilde{x}_1\\ \tilde{x}_2\\ \tilde{t}\end{pmatrix} &:= \bigvee_{m=0}^{1}:\bigvee_{n=0}^{1}:\bigvee_{o=0}^{1}: L\varepsilon_j^k\begin{pmatrix}x_1+1-2m\\ x_2+1-2n\\ t+1-2o\end{pmatrix} \\ &> 0 \cap L\varepsilon_i^{k+1} \notin L\varepsilon_l^{\kappa} : \kappa \in [0,k+1] \end{aligned} \qquad (18)$$

The points in the $\varepsilon(x_1,x_2,t)$-field are scanned at the step k+1 by application of a 6-point stencil to all points in the list $L\varepsilon^k$, while checking if the identified new points (ε>0) had been scanned by a former step. The procedure is repeated till the successor of the last lists remains empty.

With the information about the integral void fraction of a bubble, scanned in the $\varepsilon(x_1,x_2,t)$-field by the WMT, Eq.(18), with the expected value of the rising velocity of this structure, Eq.(5), and with the spatial resolution of the sensor, Δx_1, Δx_2, the bubble volume V_B^0 writes at physical standard condition for p^0, T^0:

$$\begin{aligned} V_B^0 &= \frac{p}{p^0}\frac{T^0}{T}\Delta x_1 \Delta x_2 \cdot \Delta_W \cdot \sum_{\{V_B\}}\varepsilon \cdot \left|\frac{1}{\delta} + \int_{\tau_{\delta-1}}^{\tau_\delta}\tilde{\tilde{p}}dt\right| \\ &= \frac{p}{p^0}\frac{T^0}{T}\Delta x_1 \Delta x_2 \cdot \Delta_W \cdot \sum_{\{V_B\}}\varepsilon \cdot \left|\frac{1}{\delta} + \frac{1}{2\delta(\delta+1)}\right| \end{aligned} \qquad (19)$$

It has to be noted that the first formulation of the bubble volume is of general validity. The second line is based on the assumption that $\tilde{\tilde{p}}_u$ is constant distributed over the velocity class U_δ, yielding that the mean value is given by u_δ+0.5 U_δ. For any approximation of the velocity distribution within a measurable class-width U_δ higher in order the first line of Eq.(19) has to be considered.

The presented research work concentrates basically on two-phase bubbly flow, where bubbles are ranging in diameter between 4 and 7mm. These bubbles are under experimental conditions spherical or show only a slight tendency for ellipsoidal distortion (lg(Mo)~-14,Ev~1). The volume V_B^0 at standard conditions has been expressed by the diameter d_B, supposing a spherical shape (notation: $d_{B,sph}$). A distribution function f_B is introduced by Eq.(20) that allows to calculate the expected bubble diameter $E(d_{B,sph})$ at a certain location (x_1,x_2):

$$f_B(d_{B,sph}) = \left[\frac{\partial P(d_{B,sph} < D_B)}{\partial d_{B,sph}}\right] \quad (20)$$

The local gas volume flux can be evaluated from information about local instantaneous true gas velocity and simultaneous measured void fraction by Eq.(21):

$$< u_G > (x_1, x_2) = \varepsilon(x_1, x_2, t) \cdot u_G(\varepsilon(x_1, x_2, t)) \quad (21)$$

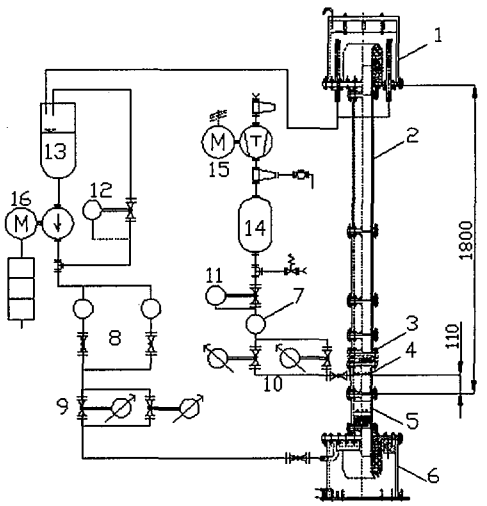

Figure 6 – Test facility

TEST FACILITY

The electrode-mesh tomograph (Fig.1) have been applied for studies on developing co-current bubbly flow at atmospheric conditions, realized with the test facility that is illustrated by Fig.6.

The rectangular channel (2) has a cross-section of 20x100mm over the length of about 55 hydraulic equivalent diameter. The channel is made from acrylic glass and modular in design, so that the WMT (3) can be set at locations every 100mm downstream the strainer unit (4).

The channel is supplied with water from a lower plenum (6) that is flooded by a circular drilled distribution pipe. Water is accelerated through a 3-dimensional shaped inlet nozzle. It is followed downstream by a strainer unit (5), where blades of 0.8mm thickness, fixed in 5mm distance, homogenize the velocity profile in x_1, x_2 direction. Also contained in the strainer unit (6), there is a sieve for turbulence profile homogenization (stainless-steel wire-mesh, 0.5mm mesh size, 1.5 hydraulic diameter downstream the strainer-blades).

Air is injected through steel needles, which are supplied through the channel wall of the air injection unit (4), 110mm downstream the turbulence sieve. The needles have an outer diameter of 2mm and a precisely drilled hole of 1.0mm diameter in their wall, pointing in x_3 direction. The needles are inserted into the channel through steel-sockets, which are mounted at the wall and fit the size of the air injection needles perfectly. The surface inside the channel is absolutely planar and smooth. The connection between air injection needles and sockets is sealed outside the channel by use of a rubber package that allows a positioning of the air injection needle with about 1mm accuracy in x_1-direction. The closest distance of the air injection hole to the wall is also approximately 1mm. There are 5 sockets in x_2-direction mounted at the channel wall at x_2=10,30,50,70 and 90mm on each side of the channel wall.

The outlet of the testing-channel was realized as an upper plenum (1) consisting of a diffuser and two suction pipes. The suction pipes are 1" in diameter and adjustable in their height. Water flows from the upper plenum (1) into a container (13) by gravity. The storage container (13) is used to separate the head for the centrifugal-pump (16) hydraulically from the outlet-condition of the channel to avoid pressure oscillations.

Water volume flow is controlled by use of two parallel switched control valves (9), sized 1:10 in their nominal flow rate. The pressure upstream the control valve block (9) is kept constant by an overflow pressure regulator (12). The flow rate is measured by a 2 stage orifice cascade (8). The flow rate can be detected with an average accuracy of approximately 2.5%. It is possible to keep the flow rate constant over the test series within about 1% shift.

The air for bubble generation was supplied by an oil-free piston compressor (15). In order to avoid pressure fluctuations, a pressurized vessel (14) have been utilized. To keep the air pressure upstream the control valves (10) constant a pressure regulator (11) have been installed. The control valves block consist of 2 parallel needle valves, sized 1:10 in their nominal flow rate. The flow rate of the air is

measured upstream the control valves in a zone of constant pressure by use of a laminar-flow-meter. The volume flow can be detected with approximately 1.5% accuracy. The amount of air is sufficient to realize superficial velocities of up to 5cm/s.
During all experiments referred in this paper the electrode-mesh sensor have been installed 480mm downstream the strainer unit (6), i.e. 470mm downstream the injection needles.

RESULTS AND DISCUSSION

The verification of the proposed methods was carried out by use of extensive testing series: a first one to study the general void fraction measurement according the proposal by Prasser at al. [5], aiming the localization of a single bubble as well as studies on the probability distribution of the void fraction. Based on this elementary study, the validity of the proposed method for the evaluation of the local true gas velocity has been investigated in a second experimental series. In a final experimental series, the obtained data for the local true gas velocity the flow field were reconstructed in space, the volume flow was calculated and compared from data supplied by a laminar flow meter. Table **1** gives an illustration over the experimental settings used in the third and below discussed series.

Table 1 Experimental conditions.

		Series No.1	Series No.1
Injection needle coordinates in (x_1,x_2)	[mm]	[(10,10),(10,30),(10,50),(10,70),(10,90)]	[(10,10),(10,30)]
WMT position downstream strainer	[mm]	480	480
Applied overall sampling rates, f_W	[Hz]	500, 800, 1000, 1200	500, 800, 1000, 1200
Superficial velocity range, gas, $<U_G>$	[mm/s]	0.5 .. 10.0	0.5 .. 10.0
Superficial velocity range, water, $<U_W>$	[mm/s]	0 .. 200	0 .. 200

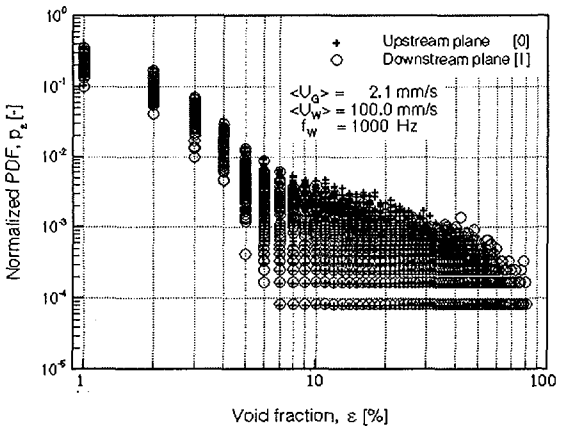

Figure 7 – Void fraction frequencies

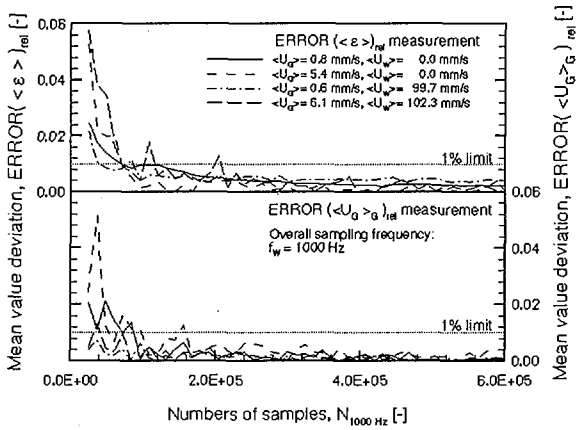

Figure 8 – Certainty in prediction of statistical momentum

Sparkling experiments

Aim was to clarify the order the noise level in the signal have to be imagined as well as to study its dependency from superficial gas and liquid velocities. Furthermore the necessary sampling duration should had been investigated in order to ensure a predefined certainty for the evaluation of various mean values.

A typical void fraction probability function is illustrated in Fig.7. The superficial velocity of the gas was $<U_G>$=2.1mm/s and the superficial liquid velocity was $<U_W>$=100.0mm/s with an overall sampling rate of f_W=1000Hz. A log-log plot has been chosen to enlarge the area of low void fractions. It is obvious that the entire p.d.f. is characterized by 2 zones (Fig.7): Void fraction level lower 7% occur often, independent from the measuring point. This region is supposed to result from the action of different electromagnetic fields around the sensor. The signal is identical with signals measured during a single phase experiment. The value of ε=7% was found as independent from $<\varepsilon>$ and f_W. The second zone in Fig.7 can be identified by the field that is approximately equally distributed at void fraction values higher 7%. The minimum for the PDF level of $p_\varepsilon=10^{-4}$ results from 10.000 sampled data-points. Maximum reached void fractions are in the order of 70~80%. The shape of this field has been found as slightly dependent on $<\varepsilon>$. Large values of $<\varepsilon>$ yield

higher void fractions (ε_{max}=70-80%). The reason therefore is seen in a reduction in lateral mobility of bubbles, which come more and more in an ancient region of the wires.

The influence of the sampling number on the calculation of mean values have been studies. For this purpose the behavior of the void fraction and true bubble rising velocity mean values, calculated by use of the above introduced algorithms, have been studies. The deviation of the superficial mean value, achieved with a limited sampling number from the true mean value, which is given per definition for $t \rightarrow \infty$, is plotted in Fig.8 for a wide range of flow condition. It can be that the relative difference of the calculated values for ε and $\langle U_G \rangle_G$ from a value obtained for very large sampling times falls to a certain level lower than 1% and remains oscillating for increasing time. In the case of high superficial, the sampling number depending mean values of the local void fraction oscillates with about 0.5% around the mean value. Lower superficial gas velocities yield an oscillation free convergence. The behavior of the mean value for the true gas velocity seems to be less depending on the cross sectional void, since independent from the flow condition all mean values oscillates for long time with an amplitude of about 0.25%.

Based on this investigation, the minimal sampling duration have been fixed appropriately in order to ensure a certainty in the measured value of more than 99%.

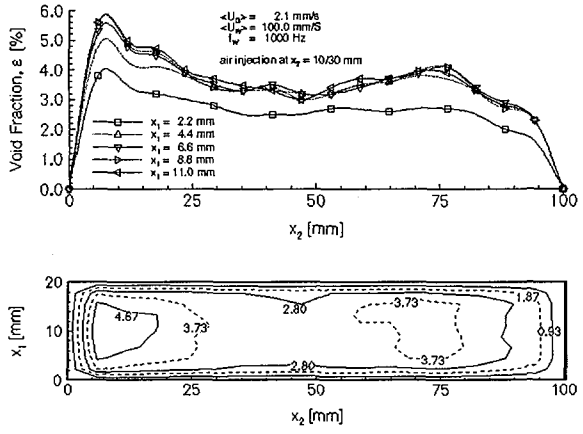

Figure 9 – Time averaged void fraction

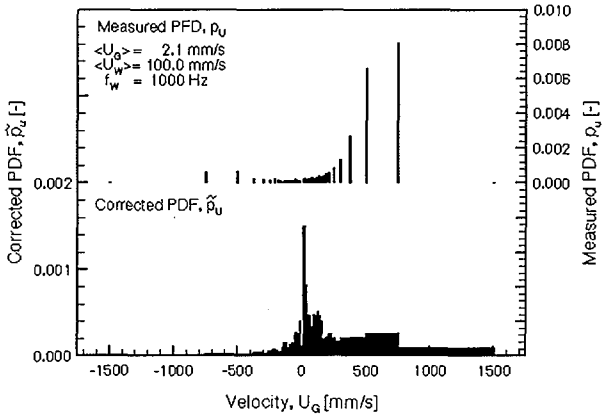

Figure 10 – Delay time p.d.f., measured and corrected

Since data for the void fraction are locally and time dependent available graphs can be provided for the instantaneous and the time averaged void fraction distribution. An example of the local time-averaged void fraction distribution is given in Fig.9 (non-symmetric air injection, No.2 in Table 1, $\langle U_G \rangle$=2.1mm/s, $\langle U_W \rangle$=100.0mm/s, f_W=1000Hz). At the channel walls the void fraction is naturally zero. A significant maximum of the void fraction (ε~6%) on the left-hand-side can be seen, corresponding with the locations of the air injection needles.

Velocity measurement

The evaluation of the local true gas velocity has been carried out according Eqs.(4)-(15). Single bubbles as well as collectives of them were sparkled into the channel. The bubbles had a diameter of approximately 2~7mm. The data supplied by the electrode-mesh device have been analyzed in order to obtain the delay time distribution, Eq.(9). An example is shown in Fig.8 ($\langle U_G \rangle$=2.1mm/s, $\langle U_W \rangle$=100.0mm/s and f_W=1000Hz). The discreet function p_t is plotted over the logarithmic stretched arguments (classes T_i) in order to obtain equidistant velocity classes. The delay-time based p.d.f., according Eq.(9), have been redistributed by Eqs.(10)-(13). The obtained velocity classes are equidistant and plotted in the lower half of Fig.10. The arguments U_i are corresponding to the delay-time classes T_j used for the plot in the upper half of Fig.10. It can be seen that the velocity based function p_u is flatter than p_t in a region of high velocities. In an area of low velocities the function p_u reaches higher level than p_t – a result of the summation of delay time classes T_j that belong to the same velocity class U_i.

Mean values for true gas velocities at different flow condition measured by the WMT, $U_{G,WMT}$, are plotted vs. the velocities $U_{G,video}$, obtained by the Video Image Processing Technique in Fig.11 for U_G=200-450mm/s and f_W as parameter..

There is a general good agreement of all data. Higher true gas velocities U_G scatter more. For data obtained with $f_W \geq 1000$Hz agreement can be confirmed within a 5% margin.. A sampling rates of lower than 800Hz have to be considered as insufficient for velocity evaluation in the studied parameter range.

In Fig.11 the uncertainty-bars for some of the measured velocity values are shown (standard deviation of u_G). The order is 5-10% of the indicated bubble rising velocity U_G. The video measured data and the values predicted by the WMT are of same order. The quality of the velocity distribution approximation by introduction of the interclass distribution function $\tilde{\tilde{p}}_u$ in 1st order can be stated as good.

An illustration of further measurement possibilities is given by Fig.12, where velocity data of an experiment with $<U_G>$=2.1mm/s and $<U_W>$=100.0mm/s are shown for a non-symmetric gas injection (series No.2 according Table 1). To give a realistic picture of the gas velocity distribution, the bubble repetition frequency has to be shown in the diagram, as well. By doing so it can be distinguished clearly, if the expected interval wherein the velocity will range is due to a real physical behavior (i.e. action of turbulence), or due to a limited number of available data.

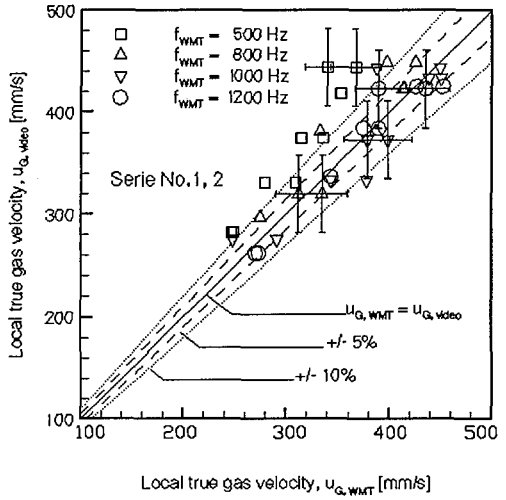

Figure 11- Quality of $U_{G,G}$ evaluation

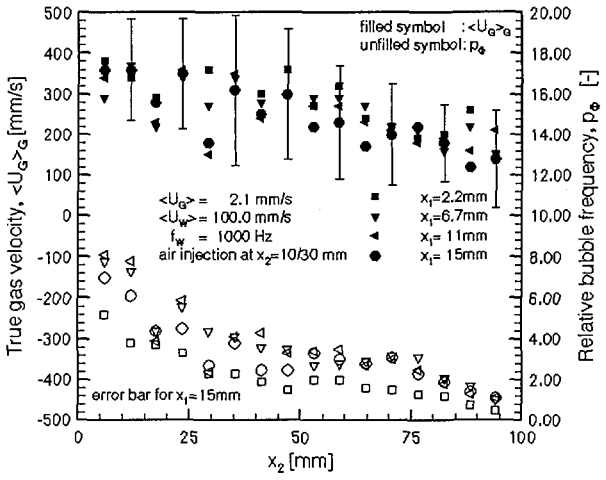

Figure 12 – $U_{G,G}$ distribution in A_c

Bubble diameter and volume flow

With the evaluated information about the local instantaneous gas velocity, there is the possibility of bubble volume reconstruction, as demonstrated by Eqs.(17)-(19). With the assumption that the bubble shape is approximately spherical, this volume can be converted into an equivalent bubble diameter and a corresponding p.d.f., f_B, Eq.(20). An example of evaluated experimental data is illustrated by Fig.11 of the above cited experiment. A significant peak value can be seen at approximate d_B=5.5cm. The bubble diameter mean value as well as the expected interval, determined by the standard deviation, are given. Also uncertainty-bars of the p.d.f. are shown. From Eq.(19) it follows directly that the evaluated diameter is directly proportional to the indicated velocity. In Eq.(19) the mean value of $\tilde{\tilde{p}}_u$ within U_δ have been used to evaluate the true rising velocity and thereby the true bubble volume.

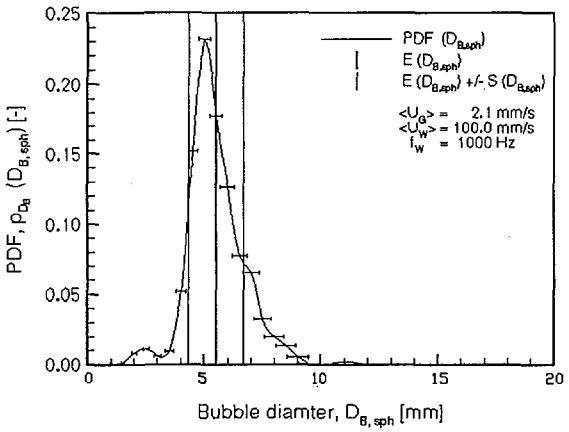

Figure 13 – Bubble diameter spectrum

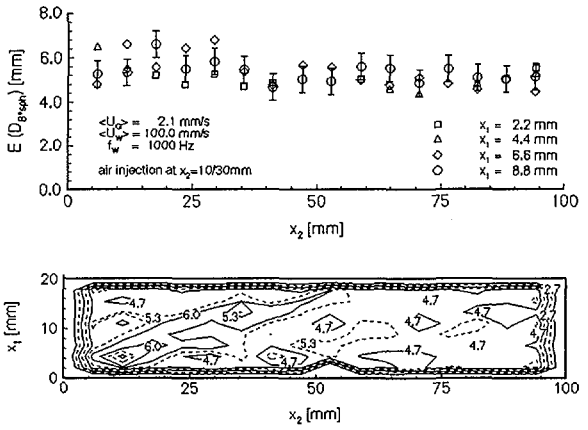

Figure 14 – Bubble diameter distribution

The possibility to plot the evaluated bubble diameters d_B in their spatial distribution over the cross-section A_c have been realized in Fig.14 for the above described experiment with an non-symmetric air-injection ($<U_G>$=2.1mm/s, $<U_W>$=100.0mm/s and f_W=1000Hz). It can be seen from Fig.14 that the bubble diameter is approximately constant distributed over A_c.

Since there are practical difficulties to obtain data of the bubble diameter from alternative experiments, the volume flow has been chosen as a suitable criterion to assess the quality of the reconstruction of bubble size in connection with the prediction of the velocity

(wherefore the accuracy was discussed independently). By use of Eq.(21) the local volume flow and its equivalent in the flux velocity can be calculated. For the cited experiment, the local distribution of the superficial velocity over A_c is shown in Fig.15. Two strong maxima can be identified in the region of air injection (x_2=10,30mm). The volume flux outside this region is neglectable small. Furthermore, there is a connection between Fig.15 and the bubble diameter- as well as local the gas velocity distribution, given by Fig12 and Fig.14, respectively: The volume flow reaches maximum values in region, where big bubbles migrate at high true velocities.

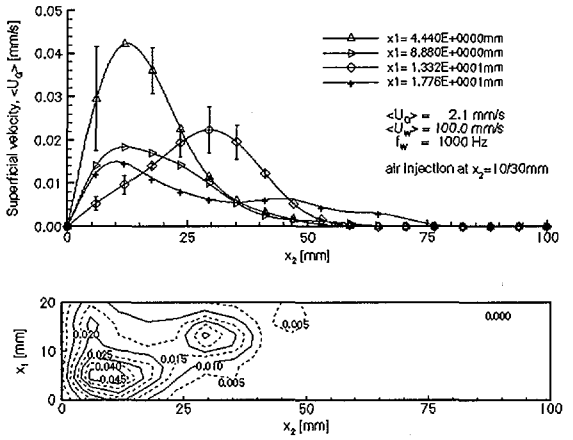

Figure 15 – Volume flux distribution

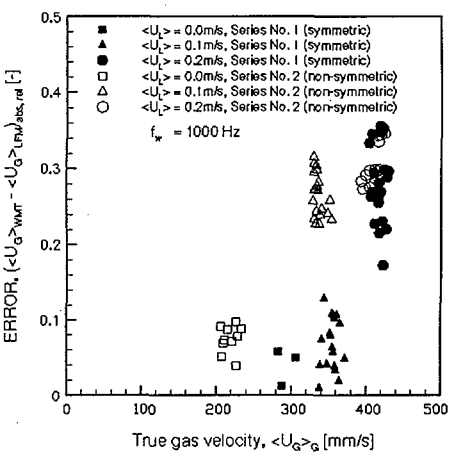

Figure 16 – Quality of $\langle U_G \rangle$ evaluation

The time and cross sectional averaged superficial velocity of the gas, $\langle U_G \rangle$, reconstructed from data supplied by the WMT, were compared to data alternatively obtained data by a laminar-flow meter, LFM. The deviation in these data is shown in Fig.16 in a plot vs. the cross-sectional and time averaged true gas velocity, $\langle U_G \rangle_G$. For low true gas velocities (<300mm/s) an error of less than 10% can be confirmed. For larger values of $\langle U_G \rangle_G$, there are relative deviations up to 30%. The reason for these errors is seen by the authors in a strong bubble deformation as well as the invalidity of the assumption that the integral-surface velocity of the bubble can be assumed as equivalent to the velocity of the approaching surface, whereon the algorithm for the evaluation of the rising velocity is based. Also obvious is that the measuring accuracy is lower for non-symmetric injected bubbles. The bubble concentration per unit volume increases for the same superficial gas velocity in the case of non-symmetric injection and so the source for a measuring error is given in a similar way than for higher superficial velocities but homogeneous bubble distribution.
To improve the accuracy of these values, there is the necessity for further extensive research.

Accuracy and certainty
Prasser et al. [5] found that the new electrode-mesh sensor is able to predict the time and sectional-cross averaged void fraction with an accuracy of approximately 1%. Furthermore there is evidence in Prasser et al. [5] that the accuracy for the local void fraction measurement is similar in order than the integral value.
The measurement of the true gas velocity is based on the analysis of the delay-time between the two signals that a migrating bubbles causes at two peripheral electrode crossing points of the WMT. For the identification of these events a change in the local void fraction ($\Phi_{\varepsilon,pos}$) is used. This event is independent from the amplitude of the void fraction signal. Insofar it can be concluded that there is theoretically no error on the measurement of the delay-time's mean value, caused by a deviation in the void fraction measurement. This is not the case for the instantaneous delay-time: a deviation in the measurement of the void fraction of one point might cause a time shift of the ramp event, $\Phi_{\varepsilon,pos}$, in the triggered signal (compare Fig.4). But if it is supposed that the error in void fraction measurement is randomly symmetrically distributed around a mean value in time and space the statistical mean value of the delay time can be correctly reflected. Evidence of this assumption have been achieved by variation of the threshold value ε_{thresh}, used to trigger the raw signal from the noise. A variation in between ε_{thresh} = 9-12% did not yield any remarkable deviation in the evaluated delay time mean value Δt. (The time and cross-sectional averaged void fractions was larger $\langle \varepsilon \rangle$=0.2%.)
Beside of the delay-time Δt, the electrode distance Δ_W is of importance. This discussion goes alone with the question of linearity in the conversion from a voltage level U_{el}, caused by the conductivity of the surrounding two-phase mixture, into a void fraction, ε. The electromagnetic field around two orthogonal spreads out wires is a very complex, 3 dimensional structure, which can not be recalculated by the obtained output signals [5]. So it is supposed, as mentioned at the very beginning, that the output signal U_{el} is a function of the average distribution of the multiphase mixture in a volume, corresponding to one mesh size (2.22 x 6.06mm). This assumption seems to be valid since the mesh size is very small and the distance in between the wires is narrow. Due to this - necessary – simplification, there is no possibility to take the wire distance or the influence of the stretched electromagnetic field into consideration.

However, the legitimacy of this assumption is confirmed by the experiments for velocity measurement (Fig.11), where no deviation of predicted gas velocity values to a certain were obviously.
The strongest source of possible deviations, uncertainty, respectively, is given by the introduction of the interclass velocity distribution $\tilde{\tilde{p}}_u$ in order to overcome the difficulties with insufficient time resolution. The PDF $\tilde{\tilde{p}}_u$ is supposed to be equally distributed within U_i. Since there is no knowledge of the real characteristics of $\tilde{\tilde{p}}_u$ the worst case has to be assumed. This situation is given if in the first case all velocities u_j , belonging to U_i, are concentrated at the lower velocity value U_i. The other case is given if all velocities u_j are concentrated at U_{i+1}. Both cases are highly unlikely, but have to be considered as possible. The result is that for velocities closed to u_{max} ($u_{max}/5$) an expected interval of up to 20% results. This uncertainty is less important for the prediction of the velocity mean value U as much more for the prediction of an instantaneous velocity u. The statistical mean value can be considered as within +/-5% correct (Fig.11), but the instantaneous value have to be assumed within the above mentioned larger interval. This is of particular interest for the calculation of equivalent bubble diameter (Fig.13) as well as volume flux (Fig.15), where the instantaneous value of the velocity is taken for calculation. Both cited figures show large uncertainty-intervals in which mean value is expected. Especially the plot of the superficial velocity distribution $<U_G>$ over the cross section A_c in Fig.15 illustrates this effect: in regions of low flux value ($(<U_G>) <$ 1mm/s), resulting from slow gas velocities (bubble diameters are approximately equally distributed over A_c) are less influenced by $\tilde{\tilde{p}}_u$ since the temporal resolution of the sensor is sufficient (interval about 3%). Areas of high flux values ($(<U_G>) >$ 3mm/s) are characterized by large uncertainties, (~10%) resulting from the approximation of the true velocity probability function p_u by use of $\tilde{\tilde{p}}_u$.
So it is not surprisingly that the prediction of the gas volume flow at standard condition suffers high deviation from the alternatively supplied data. As illustrated in Fig.16, the standard volume flow, expressed by the superficial velocity is reconstructed with a deviation lower 10% for bubble rising velocities, where the temporal resolution of the sensor is sufficient as well as the assumption of constant rising velocity is valid. Furthermore it have to be noted that an error occurs due to the slice-wise reproduction of a bubble in regions of higher rising velocities: as higher as faster as the bubble migrates as rougher the approximation of volume reconstruction according Eq.(19) seems to be. It have to be stated that the applicability of the sensor to volume flow modeling is lost for rising velocities higher than 300mm/s, where errors of about 30% were found. However, the authors sharing the opinion that these values will be significantly improved with further hardware development.

SUMMARY

A new electrode-mesh device has been applied to studies on bubble flow. Extensive data processing methods have been developed that offers the possibility to evaluate the local instantaneous void fraction, bubble rising velocity and bubble volume as well as their time and cross-sectional averaged values. These averages were used to conclude on the local distribution of the superficial gas velocity. The proposed algorithms have been applied to bubble flow in a rectangular channel ($<U_G>$=0-5mm/s,$<U_W>$=0-25mm/s and two air injection configuration). Accuracy in the prediction of void fraction was found within 5% by comparison with VIP supplied data. The reconstructed volume flow showed uncertainties in the order of up to 10% for true gas velocities lower 300mm/s and up to 30% above.

NOMENCLATURE

A_C	Cross section	1 m²
C_0	Distribution coefficient	-
D	Standard deviation	-
d_B	Bubble diameter, spherical	1 m
D_B	Bubble diameter class	1 m
E	Mean value	-
f	Probability density function	-
f_W	Wire Mesh Tomograph, WMT, overall sampling rate	1 Hz
i,j,k,l,m,n ,o	Counting variables	-
$<u_G>$ $<U_G>$	Superficial velocity of the gas (instantaneous/ time averaged)	1m/s
L	List	-
N	Number	-
p	Pressure	1 Pa
p	Probability density function, general	-
$\tilde{p}_u$	p.d.f. for equidistant velocity classes	-

$\tilde{\tilde{p}}_U$	p.d.f., locally restricted	-
P	Distribution function	-
$\vec{r}, \vec{s}$	Vectors in space R^3	1 m
t	Time	1 s
T_i	Time class	1 s
T	Temperature	1 K
U_{cl}	Voltage	1 V
u, U	True velocity (instantaneous,time averaged)	1m/s
U_i	Velocity class, general	1m/s
$\tilde{U}_i$	Velocity class, equidistant	1m/s
V_B	Bubble volume	1 m^3
x_1, x_2	Coordinates in the cross-section	1 m
Φ	Ramp event	-
ε	Void fraction	-
δ	Delay frames	-
Δ_W	Distance between measuring planes	1 m

Superscript

^{0}	Normalized or referring standard condition
^{A}	Referring air
$^{k,\kappa}$	List counter
^{W}	Referring water

Subscript

$_\delta$	Referring delay frame number
$_\varepsilon$	Referring void fraction
$_B$	Referring bubble
$_{i,j,k,l,m,n,o}$	Counting variables
$_{LFM}$	Referring laminar flow meter
$_{max}$	Maximum
$_{req}$	Required
$_{sph}$	Spherical (equivalent)
$_{thresh}$	Threshold
$_T$	Referring time delay
$_U$	Referring velocity
$_{Video}$	Referring video
$_{WMT}$	Referring Wire-Mesh Sensor
$_{X1, X2}$	Referring coordinates in the cross section

REFERENCES

[1] Hori, K., Fujimoto, T., Kawanishi,H., Nishikawa,H., Advanced high speed X-ray CT scanner for measurement and visualization of multi-phase flow. In: *OECD/CSNI Specialist meeting on Advanced Instrumentation and Measurement Techniques*, Santa Barbara, USA, March 17-20, 1997.

[2] Kataoka,I., Serizawa,A. Statistical behaviors of bubbles and its application to prediction of phase distribution in bubbly two-phase flow. In: *The International Conference on Multiphase Flows '91,* Tsukuba, Japan, September 24-27, 1991, 459-461.

[3] Mercier,J., Lyrio,A., Forslund,R. Three-dimensional study of the non-rectilinear trajectory of air bubbles in rising water. *Transaction of the ASME - Journal of Applied Mechanics*, 1973, 650-654

[4] Prasser, H.-M., Böttger, A., Zschau, J., A new electrode-mesh tomograph for gas-liquid flow. *Flow Measurement and Instrumentation*, 1998, **9**, 111-119.

[5] Reinecke,N., Mewes,D., Recent developments in industrial research application of capacitance tomography. *Measurement Sci. Technol.*, 1997, **7**, 233-246.

[6] Sadatomi,M., Sato,Y. Two-phase flow in vertical non-circular channels. *Int. J. Multiphase Flow,* 1982, **8**, 641-655.

[7] Zuber,N., Findlay,J.A., Average volumetric concentration in two-phase flow systems. *J. Heat Transfer*, 1965, **87**, 453-468.